Vietnam Journal of Science and Technology ***64***(2) (2026) 267–279
DOI: https://doi.org/10.15625/2525-2518/20030

6β-hydroxygeniposide, a potent α-glucosidase inhibitor from *Gardenia jasminoides* growing in Viet Nam

Vu Dinh Hoang[1,*], Nguyen Khac Hung[1], Pham Quang Duong[2], Nguyen Thi Viet Thanh[1], Dinh Thi Phuong Anh[1], Chu Van Tan[3], Cao Duc Tuan[4], Tran Hong Ngoc[5], Truong Gia Bao[6], Tran Dai Lam[2]

[1]*Hanoi University of Science and Technology, 1 Dai Co Viet street, Bach Mai ward, Ha Noi, Viet Nam*
[2]*Institute of Materials Science, Vietnam Academy of Science and Technology, 18 Hoang Quoc Viet, Nghia Do ward, Ha Noi, Viet Nam*
[3]*Center for High Technology Innovation, Vietnam Academy of Science and Technology, 18 Hoang Quoc Viet, Nghia Do ward, Ha Noi, Viet Nam*
[4]*Hai Phong University of Medicine and Pharmacy, 72A Nguyen Binh Khiem, Gia Vien ward, Hai Phong, Viet Nam*
[5]*Faculty of Pharmacy, Phenikaa University, Duong Noi ward, Ha Noi, Viet Nam*
[6] *Gifted Class for Chemistry, High School for Gifted Students, Hanoi University of Science, Vietnam National University, Ha Noi, Viet Nam*

[*]Email: *hoang.vudinh@hust.edu.vn*

Received: 27 January 2024; Accepted for publication: 23 March 2024

Abstract. According to the statistics of WHO in 2019, diabetes was one of the top 10 causes of death in Viet Nam and the incidence increasing day by day has required more effective treatment methods. For a long time, natural products have played an important role in drug screening programs. *Gardenia jasminoides* belongs to the *Gardenia* genus of the Rubiaceae family, in which previous research showed potential ability in diabetes treatment through various mechanisms. In this study, 3 iridoids were isolated from *G. jasminoides* collected in Viet Nam and the α-glucosidase inhibitory activity was evaluated for the first time. The results showed that 6β-hydroxygeniposide (**2**) expressed the strongest activity with IC_{50} at 6.38 ± 0.12 μM, while geniposide (**1**) and 6α–hydroxygeniposide **(3)** were inactive. The inhibitory mechanism of 6β-hydroxygeniposide was revealed by molecular docking and molecular dynamics. 6β-Hydroxygeniposide competed and blocked p-nitrophenyl-α-D-glucopyranoside substrate reaching the reaction center of the enzyme, which was expressed through lower non-bonding interaction energy and stable binding affinity.

Keywords: 6β-hydroxygeniposide, anti α-glucosidase, diabetes, Gardenia jasminoides, molecular docking, molecular dynamic simulation.

Classification numbers: 1.2.1, 1.2.4, 4.8.5.

1. INTRODUCTION

Diabetes is a chronic disease that occurs when the pancreas produces not enough insulin or when the body does not effectively use the insulin produced. The diabetes diagnosis rate has been

increasing recently with about 1 in 17 Vietnamese adults (1 in 15 men and 1 in 20 women) having diabetes [1]. Based on causes and symptoms, diabetes is divided into diabetes type 1 and type 2. Type 1 diabetes (previously known as insulin-dependent, juvenile, or childhood-onset) is caused by insulin-produced deficiency and requires daily insulin supplements. Meanwhile, type 2 diabetes influences glucose consumption for energy metabolic pathways. It stops the body from using insulin properly without affecting insulin synthesis, which can lead to several critical complications in the body, such as retinopathy, heart attack, stroke, diabetic nephropathy, and nerve damage [2]. Type 1 diabetes requires islet transplantation or daily injection with insulin, while type 2 diabetes is often preventable. Factors that contribute to developing type 2 diabetes include being overweight, not getting enough exercise, and genetics. One of the prevention therapies is to decrease glucose absorption mediated via inhibiting starch-hydrolyzing enzymes like α-glucosidase [3]. Alpha -glucosidase is located in the brush border of the small intestine, which hydrolyzes terminal, non-reducing (1→4)-linked α-D-glucose residues and releases *D*-glucose. Therefore, α-glucosidase is widely used as an effective target in diabetes treatment drug development programs.

Gardenia jasminoides belongs to the *Gardenia* genus of Rubiacea family, which is distributed in Viet Nam, Bhutan, China, India, Cambodia, Korea, and Oceania countries [4]. Previous research revealed the effects of *G. jasminoides* extract on blood sugar modulation in mouse models [5]. In particular, several iridoids isolated from *G. jasminoides* expressed anti-diabetes through various mechanisms, for instance: inducing insulin production, improving insulin signaling response, inhibiting starch degradation enzymes, etc [5-7]. Therefore, this study aimed to determine structures and evaluate α-glucosidase inhibition ability of several iridoids isolated from *G. jasmonoides in* Viet Nam.

2. MATERIALS AND METHODS

2.1. Materials

Leaves and branches of *Gardenia jasminoides* Ellis, 1761 were collected at Ninh Binh province, Viet Nam in August 2020. The sample was identified by Nghiem Duc Trong, Hanoi University of Pharmacy. A voucher specimen (NF104.01-2019.329-1) was preserved at the Center for High Technology Research and Development, Vietnam Academy of Science and Technology (VAST).

2.2. General experimental procedures

NMR spectra were recorded on a Bruker Avance 500 MHz spectrometer (Germany) at the Institute of Chemistry, VAST. Tetramethylsilane (TMS) was used as an internal reference for chemical shift calculation and coupling constants (J) are given in Hertz (Hz). Column chromatography (CC) was performed on silica gel 100 (63 - 200 μm) and C18 reversed-phase silica gel (RP-18, 15 - 25 μm), which were purchased from Merck Vietnam Ltd. TLC plates were visualized with 10% sulfuric acid combined with heating.

2.3. Extraction and isolation

The air-dried branches and leaves of *G. jasminoides* (2.5 kg) were extracted 4 times with 10 L MeOH at room temperature in combination with an ultra-sound method. The solvent was

vacuum evaporated to obtain 180 g MeOH extract. Then, the extract was dispersed in H_2O and successively partitioned with dichloromethane (*n*-hexane) and ethyl acetate (EtOAc).

The EtOAc extract was subjected to silica gel column chromatography eluting with the solvent system dichloromethane (DCM)-methanol (MeOH) (1:0 → 5:5, v/v) gradient to yield 11 fractions Fr.1→Fr.11. Fr.9 was fractionated on silica gel column eluting with DCM-MeOH (9:1 → 82:14, v/v) as eluent to yield 8 fragments (Fr.9.1→Fr.9.8). Fraction 6 (950 mg) was fractionated on a silica gel column chromatography with DCM/MeOH (9:1 → 8:2, v/v) eluent system, yielding 9 subfractions Fr.6.1→ Fr.6.9. Compound 1 (10 mg) was obtained from fraction Fr.6.8 by using silica gel chromatography eluting with DCM/MeOD/acetic acid (9:1:0.01, v/v/v). Compound 2 (6.6 mg) was obtained from Fr. 9.6 by subsequent Sephadex LH-20 chromatography with MeOH eluent. Fraction 6.4 (94 mg) was fractionated on Sephadex LH-20 with MeOH as eluent to obtain Fr 6.4.1 → Fr.6.4.5. Compound 3 (9.2 mg) was isolated from Fr.6.4.1 by preparative TLC with solvent system DCM/MeOD/acetic acid (9:1:0.01, v/v/v).

Geniposide (1): white powder. (Supplementary data: Figure S1) ^{1}H-NMR (500 MHz, CD_3OD) δ (ppm): 5.18 (1H, d, 8.0 Hz, H-1), 7.52 (1H, d, 1.0 Hz, H-3), 3.23 (1H, m, H-5), 2.11 (1H, m, H-6a), 2.83 (1H, m, H-6b), 5.81(1H, brs, H-7), 2.74 (1H, brt, 7.5 Hz, H-9), 4.31 (1H, d, 14.5 Hz, H-10), 4.19 (1H, dd, 2.0, 14.5 Hz, H-10b), 3,73 (3H, s, OMe); *β*-D-Glucopyranosyl: 4.72 (1H, d, 8,0 Hz, H-1′), 3,33 (1H, m, H-2′), 3.53 (dd, 11.0, 6.0 Hz, H-3′), 3.41 (1H, m, H-4′), 3.43 (1H, m, H-5′), 3.88 (1H, t, 11.5 Hz, H-6′a), 3.70 (1H, m, H-6′b). (Supplementary data: Figure S2) ^{13}C-NMR (125 MHz, CD_3OD) δ (ppm): 98.27 (C-1), 153.32 (C-3), 112.56 (C-4), 36.58 (C-5), 39.69 (C-6), 128.34 (C-7), 144.79 (C-8), 47.02 (C-9), 61.41 (C-10), 169.53 (C-11), 51.72 (OMe); *β*-D-Glucopyranosyl: 100.35 (C-1′), 74.87 (C-2′), 77.86 (C-3′), 73.84 (C-4′), 78.38 (C-5′), 62.66 (C-6′).

6*β*-hydroxygeniposide (2): white powder. (Supplementary data: Figure S3) ^{1}H-NMR (500 MHz, CD_3OD) δ (ppm): 5.21 (1H, d, 6.5 Hz, H-1), 7.53 (1H, s, H-3), 3.02 (1H, ddd, 1.0, 4.5, 7.5 Hz, H-5), 4.57 (1H, brs, H-6), 5.83 (1H, s, H-7), 3.06 (1H, t, 6.5, 6.0 Hz, H-9), 4.34 (1H, d, 15.0 Hz, H-10a), 4.22 (1H, d, 15.5 Hz, H-10b), 3.77 (3H, s, OMe); *β*-D-glucopyranosyl: 4.70 (1H, d, 7.5 Hz, H-1′), 3.24 (1H, dd, 8.0, 9.5 Hz, H-2′), 3.40 (1H, m, H-3′), 3.33 (1H, m, H-4′), 3.31 (1H, m, H-5′), 3.89 (1H, d, 12.0 Hz, H-6′a), 3.56 (1H, m, H-6′b). (Supplementary data: Figure S4) ^{13}C-NMR (125 MHz, CD_3OD) δ (ppm): 98.28 (C-1), 153.88 (C-3), 110.78 (C-4), 45.51 (C-5), 82.25 (C-6), 130.11 (C-7), 147.51 (C-8), 47.10 (C-9), 61.00 (C-10), 170.32 (C-11), 52.08 (OMe); 100.27 (C-1′), 74.76 (C-2′), 77.84 (C-3′), 73.79 (C-4′), 78.37 (C-5′), 62.64 (C-6′).

6*α*-hydroxygeniposide (3): white powder. (Supplementary data: Figure S7) ^{1}H-NMR (500 MHz, CD_3OD) δ (ppm): 5.07 (1H, d, 9.0 Hz, H-1), 7.67 (1H, s, H-3), 3.30 (1H, m, H-5), 3.66 (1H, d, 5.5 Hz, H-6), 6.04 (1H, s, H-7), 2.58 (1H, bt, 8.0 Hz, H-9), 4.21 (1H, d, 15.5 Hz, H-10a), 4.46 (1H, d, 16.0 Hz, H-10b), 3.76 (3H, s, OMe); *β*-D-glucopyranosyl: 4.73 (1H, d, 8.0 Hz, H-1′), 3.24 (1H, m, H-2′), 3.41 (1H, t, 9.0 Hz, H-3′), 3.36 (1H, m, H-4′), 3.32 (1H, m, H-5′), 3.62 (1H, dd, 5.5, 12.0 Hz, H-6′a), 3.85 (1H, dd, 1.5, 11.0 Hz, H-6′b).

2.4. *α*-glucosidase inhibition assay

α-glucosidase inhibition assay of isolated compounds **1-3** was performed on 96 wells following Li *et al*. [8] and Acarbose was used as a reference control. Briefly, samples were diluted with DMSO to achieve the respective concentrations in mixtures at 10, 50, 200, and 250 μM. For the control, the sample was replaced by an equal volume of phosphate buffer. The reagents include

phosphate buffer 100 mM pH 6.8; yeast α-glucosidase 0.2 U/ml, sample, and 2.5 mM p-nitrophenyl-α-D-glucopyranoside. The mixtures were incubated at 37^{o}C. After 30 minutes, the reactions were stopped with Na_2CO_3. The absorbance of the reaction was determined on a BIOTEK instrument at a wavelength of 410 nm (A). The inhibition ability was calculated as follows

$$\text{Inhibition (\%)} = 100 \times [\text{A(control)} - \text{A(sample)}] / \text{A(control)}.$$

Half maximal inhibitory concentration (IC_{50}) was calculated using Table curve software.

2.5. Molecular docking and molecular dynamic simulation

To evaluate the relationship between structure and α-glucosidase inhibition activity of isolated compounds, molecular docking, and dynamic simulation was performed following strategies and protocols described by Pathania S *et al.* [9], Shivanika C *et al.* [10], Peytam F *et al.* [11] and Ali M *et al.* [12]. The general protocols include 3 steps: (1) Docking validation, (2) Docking analyzing molecules to protein, and (3) Molecular dynamic simulation of the docked complex.

2.5.1. Docking validation

The docking procedure was validated by using two methods simultaneously: (1) re-dock and (2) ROC curve analysis. For the re-dock analysis, *Saccharomyces cerevisiae* α-glucosidase with co-crystalized α-D-glucopyranose (GLC) 3D structure (PDB ID: 3A4A) was downloaded from the RCSB protein data bank. The enzyme and GLC were separated manually by using PyMOL 2.5 (Schrödinger, ILC) and prepared for docking individually, following the manual of Autodock vina [13] and PLANTS [14] with a default setup. The grid box was defined to extract the same for both docking tools, in which the center of box coordinates (x, y, z) was set at 22.625, -8.069, 24.158, and the box size was set to 50 for each dimension [11]. These parameters were used in all the validation and isolated compounds docking. The best pose of GLC obtained from each program was used for RMSD calculated in comparison to the original crystal structure. The smaller the RMSD, the better the docked pose.

For the evaluation of the distinguishing active from the inactive compounds, receiver operating characteristic curve (ROC curve) analysis was conducted following Pathania S *et al.* [9]. Anti α-glucosidase assay screening results were downloaded from PubChem databank under AID ID: 2110, 2111, 2113, and 2115. The active compounds with $IC_{50} \leq 10$ μM were selected, which resulted in 31 inhibitors (Supplementary data: Table S1). For the decoy set regeneration, decoy ligands similar to each of the inhibitors were obtained from DUD-E online server (http://dude.docking.org/) [15]. All of 32 inhibitors and 927 decoys were docked against the active site of α-glucosidase (PDB ID: 3A4A) as following re-dock protocols by using Autodock vina and PLANTS. The area under the ROC (AUC) and *p*-value at 95 % confidence interval were calculated with GraphPad Prism 8 (Dotmatics, ILC). The higher AUC means the better the model's performance at distinguishing between the active and inactive classes [16].

2.5.2. Docking process

After the validated docking protocol, all the isolated compounds and *p*-nitrophenyl-α-D-glucopyranoside (PNG) were docked to α-glucosidase (3A4A) as following the manual. In brief, the 3D structures were downloaded from the PubChem library: geniposide (CID: 107848), 6α-hydroxygeniposide (CID: 6325021), 6β-hydroxygeniposide (CID: 442433), PNG (CID: 92969).

Hydrogens were explicitly added to 3D structures and were saved in MOL2 format. For generating energy-minimized conformers, the molecules were subjected to 10000 steps of steepest descent energy minimization with general AMBER force field (GAFF) using OpenBabel 2.3.1 software [17]. Obtained conformers were used as ligands for molecular docking as described in the PLANTS manual [14].

2.5.3. Molecular dynamics

GROningen MAchine for Chemical Simulation (GROMACS) 2021.4-2 package was used for the molecular dynamic simulation. The GROMACS solves Newtonian equations of motion for the desired system, thereby calculating how atomic coordinates vary as a function of time and testing the stability of complexes [18]. For each docked complex, independent simulation runs were performed to generate trajectories following protocols by Lemkul JA [19]. Briefly, the complex was solvated with water molecules with the TIP3P model. At physiological pH, the structures were negatively charged. To neutralize the systems, 20 Na^+ were added by replacing water molecules at positions of favorable electrostatic potential. Solvated and neutralized systems were then minimized with 50000 steps using the steepest descent method to remove close van der Waals contacts. After energy minimization, equilibration was often conducted in two phases. The first phase was conducted under an NVT ensemble (constant Number of particles, Volume, and Temperature) then NPT ensemble for the pressure equilibration was subsequently performed. Both the two stages were conducted at 50 picoseconds. Following the equilibrations was the MD simulation. The simulation was conducted with 250.000 steps with the time step dt = 0.002 (2 fs), which was 500 picoseconds (0.5 nanosecond) of simulation. System RMSD, root mean square fluctuation (RMSF) analysis of backbone and side chain, non-bonded interacting energies were calculated as the GROMACS documentation [18]. Simulated systems were collected, visualized, and aligned with PyMOL 2.5 (Schrödinger, ILC). 2D non-bond interaction diagrams were generated by $LigPlot^+$ [20].

3. RESULTS AND DISCUSSION

3.1. Structure determination

Compound **1** was isolated as a white powder. NMR data of compound **1** showed features of an iridoid glycoside. ^{1}H-NMR showed a specific signal of iridoid aglycone. Acetal proton δ_H 5.18 (d, J = 8.0 Hz, H-1) specific for H-1 of the iridoid skeleton. Meanwhile, olefinic protons at δ_H 7.52 (d, J = 1.0 Hz, H-3), δ_H 5.81 (brs, H-7) were assigned for H-3 and H-7. Oxymethylene protons δ_H 4.31 (d, J = 14.5 Hz, H-10a) and δ_H 4.19 (dd, J = 2.0, 14.5 Hz, H-10b) indicated alcohol CH_2OH attached at C-10. Besides, ^{1}H-NMR also showed an oxymethyl signal at δ_H 3.73 (s, OMe). ^{13}C-NMR, HSQC, and HMBC expressed signals of 18 carbon atoms, including 12 atoms of aglycone and 6 atoms belonging to the glycoside part. Chemical shifts δ_C 153.32 (C-3), 112.56 (C-4), 128.34 (C-7), 144.79 (C-8) were assigned for double bonds C-3/C-4 and C-7/C-8 of a 10-carbon skeleton iridoid. The chemical shift of sp^3 methylene δ_C 39.69 (C-6) belonged to the C-6 position. Anomeric proton δ_H 4.72 (d, J = 8.0 Hz, H-1′) together with specific chemical shifts δ_C 100.35 (C-1′), 74.87(C-2′), 77.86 (C-3′), 73.84 (C-4′), 78.38 (C-5′) and 62.66 (C-6′) indicated the presence of a β-D-glucopyranosyl moiety. From these findings and comparing them with the literature data, compound **1** was determined to be geniposide (Figure 1) [21].

Compound **2** was isolated as a white powder. NMR spectra of compound **2** suggested an iridoid glycoside. ^{13}C-NMR, HSQC, and HMBC expressed signals of 17 carbon atoms, including

11 atoms of aglycone and 6 atoms belonging to the glycoside moiety. Chemical shifts at δ_C 153.88 (C-3), δ_C 110.78 (C-4), δ_C 130.11 (C-7), δ_C 147.51 (C-8) were assigned for specific double bonds C-3/C-4 and C-7/C-8 of a 10-carbon skeleton iridoid. The alcohol functional group δ_C 61.00 (C-10) was determined at C-10 meanwhile, the acetyl group attached to C-4. ^{1}H-NMR spectra showed 02 specific olefinic protons for H-3, H-7 at δ_H 7.53 (s, H-3) and δ_H 5.83 (brs, H-7); 01 acetal proton at δ_H 5.21 (d, J = 6.5 Hz, H-1). Two geminal coupling protons δ_H 4.34 (d, J = 15.0, H-10a); δ_H 4.21 (d, J = 15.5 Hz, H-10b) indicated the presence of CH_2OH at C-10. ^{1}H-NMR also revealed 01 oxymethyl proton δ_H 3.77 (s, OMe) and 01 β-OH proton δ_H 4.57 (brs, H-6). The presence of anomeric proton δ_H 4.70 (d, J= 7.5 Hz, H-1′), 06 protons within the range 3.2-3.8 ppm, and specific carbon signals confirmed the presence of β-D-glucopyranosyl moiety (Table 1). This monosaccharide is attached to the aglycone at the C-1 position, which was verified by a cross peak between H-1′ and C-1 (δ_C 98.28) on HMBC. Compared with previous articles, compound **2** was identified to be 6β-hydroxygeniposide or scandoside methyl ester (Figure 1) [22].

^{1}H-NMR data of compound **3** were similar to those of compound **2**, an iridoid glycoside. Two olefinic protons δ_H 7.67 (s, H-3) and 6.04 (s, H-7) were assigned for specific H-3, H-7, respectively; an acetal proton at H-1 δ_H 5.07 (d, 9.0, H-1) of the iridoid skeleton. Oxymethyl signal appeared at δ_H 3.76 (s, OMe). The alcohol group at C-10 was confirmed by the presence of two oxymethylene protons δ_H 4.21 (d, J = 15.5 Hz, H-10a) and δ_H 4.46 (d, J = 16.0 Hz, H-10b). The anomeric proton δ_H 4.73 (d, J = 8.0 Hz, H-1′) together with 6 specific protons chemical shifts from 3.25-3.88 ppm indicated the presence of a β-D-glucopyranosyl. However, the H-6 proton gave a doublet signal with a coupling constant J = 5.5 Hz suggesting a α-OH configuration at C-6. From these findings and comparing them with the literature data, compound **3** was determined to be 6α-hydroxygeniposide (Figure 1) [23].

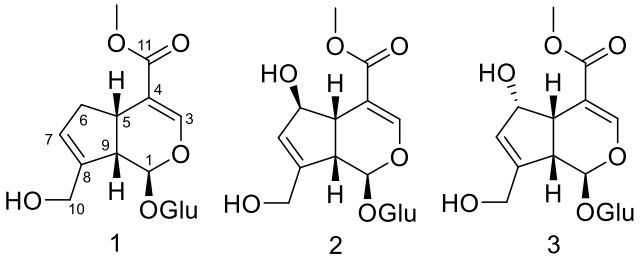

Figure 1. Structure of isolated compounds **1-3**.

3.2. α-glucosidase inhibition of isolated iridoids

Isolated iridoids were examined for the anti α-glucosidase ability. The results showed that although having similar structures, their inhibition activity was significantly different. 6β-hydroxygeniposide (**2**) strongly inhibited the α-glucosidase with IC_{50} = 6.38 ± 0.12 μM, meanwhile, 6α-hydroxygeniposide (**3**) and geniposide (**1**) were inactive (Table 2). Especially, the differences between isolated iridoids are only at the C-6 position (Figure. 1). To understand the effects of C-6 substitute groups on the inhibition activity of isolated compounds, molecular docking and dynamic simulation were conducted.

3.3. Molecular docking and dynamic simulation

Molecular Dynamics (MD) simulations is a computational method that employs Newton's laws to evaluate the motions of water, ions, small molecules, and macromolecules or more complex systems. The MD can give a reliable view of how ligands interact with protein; the binding model and relative binding energy can be calculated [24]. For the unknown complex, molecular docking is often chosen as the starting structure in MD. However, a good starting structure can reduce the cost of molecular simulation. Therefore, several methods are used to validate the accuracy of docking protocol such as RMSD calculation of re-dock with a co-crystallized ligand or ROC curve analysis of active and decoy sets [25].

3.3.1. Docking validation

Docking results extremely depend on the algorithm and scoring function of each software. To ensure the objectivity of the docking process and get the best pose structure for molecular dynamics, two well-known docking tools were used. Autodock vina was developed by Oleg Trott [13], working based on a gradient descent algorithm. Meanwhile, the PLANTS used Ant colony optimization algorithms, a probabilistic technique for solving computational problems that can be reduced to finding good paths through graphs [14].

Table 1. Validation of docking protocols.

Protocol	Redock analysis	ROC curve analysis	
	RMSD (nm)	AUC	*p*-value*
Autodock vina	0.249	0.6371	0.0124
PLANTS	0.554	0.6545	0.0063

**p*-value were calculated at 95 % confidence interval.

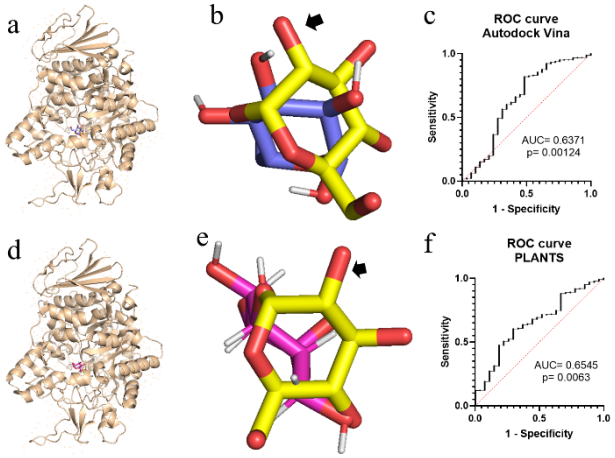

Figure 2. Redocking of α-D-glucopyranose to *S. cerevisiae* α-glucosidase (PDB ID: 3A4A) and ROC curve analysis of Autodock vina (a, b, c) and PLANTS (d, e, f) tools. (a), (d): docking pose; (b), (e): co-crystalized (indicated by arrows) and re-docked poses of GLC.

The re-dock of co-crystalized α-D-glucopyranose (GLC) to *Saccharomyces cerevisiae* α-glucosidase (PDB ID: 3A4A) showed that Autodock vina had a smaller RMSD value compared to PLANTS, (0.249 and 0.554 nm, respectively). However, the ROC curve revealed PLANTS docking tool was more reliable in distinguishing the active and inactive compounds, which was

indicated by the higher area under the ROC (AUC) (Table 1, Figure 2). Besides, a small *p*-value at 95% confidence interval also demonstrated the accuracy of the docking method (Table 1). Therefore, the PLANTS was used for generating the initial structures of isolated iridoids to α-glucosidase (PDB ID: 3A4A).

3.3.2. Molecular dynamic

Premier docking results showed that 6β-hydroxygeniposide had the lowest docking score (Table 2), indicating that it might have a higher binding affinity to the enzyme than other compounds. Although the difference in docking score of 6β- and 6α-hydroxygeniposide is not considerable, simulation results revealed the distinction of molecular dynamics between these two compounds.

Table 2. Anti α-glucosidase activities (IC_{50}), docking score, and systems RMSD of isolated iridoids.

	Geniposide	6β-hydroxygeniposide	6α-hydroxygeniposide
Anti α-glucosidase (IC_{50} μM)	I*	6.38 ± 0.12	I
PLANT score	-66.2304	-86.7515	-79.7794
RMSD (nm)	0.7029 ± 0.3666	0.1507 ± 0.0300	0.2017 ± 0.0355

*I: Inactive.

With the highest RMSD value, the geniposide-enzyme complex showed extremely high inconsistency during the simulation, which means that the complex was not stable and the connection between geniposide and *a*-glucosidase was weak. By the end of the simulation, geniposide was recorded to appear outside of the binding cavity in comparison to 6α- and 6β-hydroxygeniposide (Figure 3(a)). Root mean square fluctuation (RMSF) analysis of backbone and side chain residues of the enzyme also expressed high variation around amino acids 230 -250 and 430-450, which belong to the reaction center of *a*-glucosidase [26] (Figure 4, Supplementary data: Tables S4, S5). Non-bond interacting energy analysis of geniposide-enzyme complex during the end period of simulation (from 300-500 ps) almost reached 0 kJ/mol which indicates that there was no interaction between geniposide and the enzyme (Figure 7).

These results might explain the inactivity of geniposide in anti α-glucosidase assay, in which the geniposide could not approach the reaction center due to its thermodynamic state. Therefore, the enzyme was not affected by the presence of geniposide, which meant that the reaction center was free and the catalysis happened (indicated by the high fluctuation of residue in the cavity pocket, Figure 4).

On the other hand, both 6α- and 6β-hydroxygeniposide were bound to the enzyme at the reaction center during the whole time of simulation. However, the fluctuation in amino acids zones 230 -250 and 430-450 of 6β-hydroxygeniposide was lower than in 6α-hydroxygeniposide (Figure 4, Table 2). Besides, alignment showed 6β-hydroxygeniposide-enzyme complex position was slightly different from X-ray structure in comparison with 6α-hydroxygeniposide (Figure 3). Non-bond linkage analysis also revealed that the difference in C6-OH configuration changed the binding conformers of the two compounds. 6β-hydoxygeniposide was connected with the enzyme through more non-bond interactions than 6α-hydoxygeniposide (Figure 5, Supplementary data: Table S2).

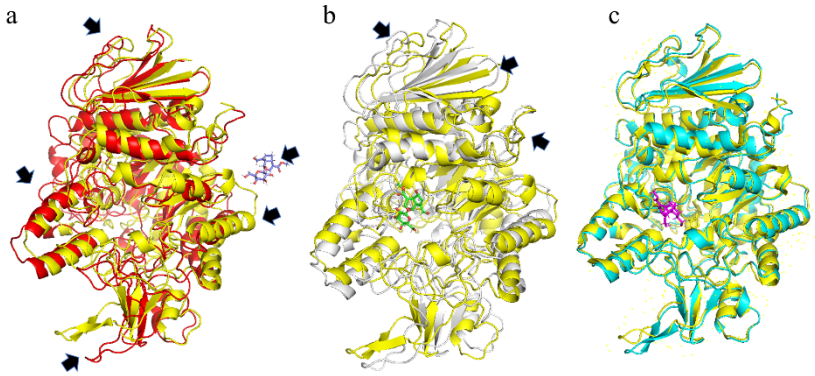

Figure 3. Positions of (a) geniposide, (b) 6α-, (c) 6β-hydroxygeniposide and α-glucosidase (3A4A) by the end of the simulation (at 500 picoseconds) are aligned with x-ray structure of the enzyme. Arrows indicated the difference between simulation and x-ray structure.

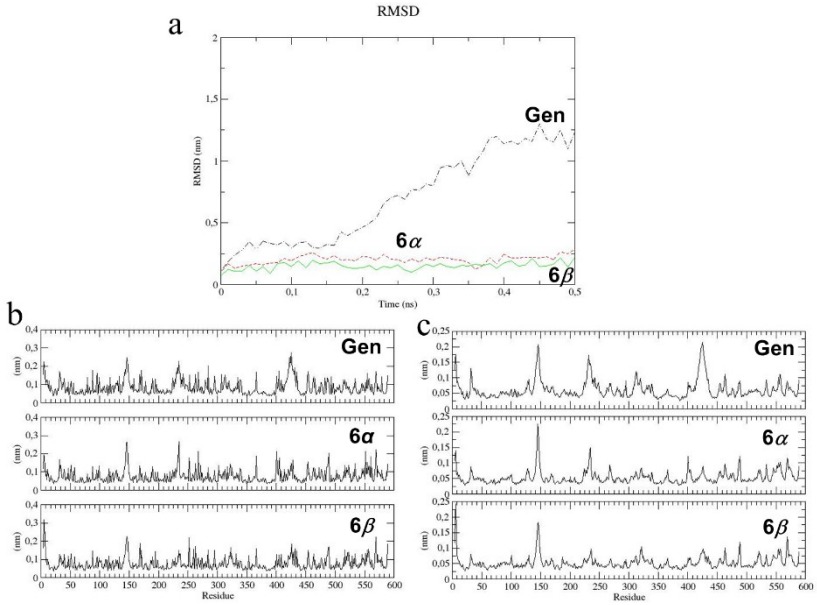

Figure 4. RMSD analysis geniposide, 6α-, 6β-hydroxygeniposide and α-glucosidase (3A4A) complexes during simulation (500 picoseconds) (a) Root mean square fluctuation (RMSF) analysis of backbone (b) and side chain residues (c) gen: geniposide; 6α: 6α-hydroxygeniposide; 6β: 6β-hydroxygeniposide.

Further analysis and alignment of simulated 6α-, 6β-hydroxygeniposide, and *p*-nitrophenyl-α-D-glucopyranoside (PNG, the substrate in anti α-glucosidase assay) complexes showed that both the iridoids bound to the enzyme at the same position as PNG (Figure 6). However, the non-bonding interacting energy analysis exhibited significant differences. Overall, the interaction energies of 6β-hydroxygeniposide were lower throughout the whole simulation time (Figure 7). In addition, the average total energy of 6β-hydroxygeniposide was the lowest as compared with PNG and 6α-hydroxygeniposide (Table 3). These obtained results were compatible with the non-bond linkage analysis above. The more interactions are, the stronger interacting energy is. Especially, analysis results showed that there was no distinguishable difference in the total interaction energy between 6α-hydroxygeniposide and PNG (Table 3).

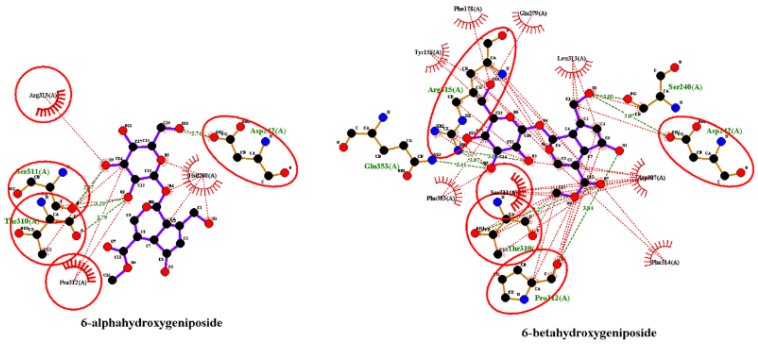

Figure 5. 2D non-bond interactions analysis of 6α- and 6β-hydroxygeniposide. Circle expressed similar amino acids joined in interacting between two complexes.

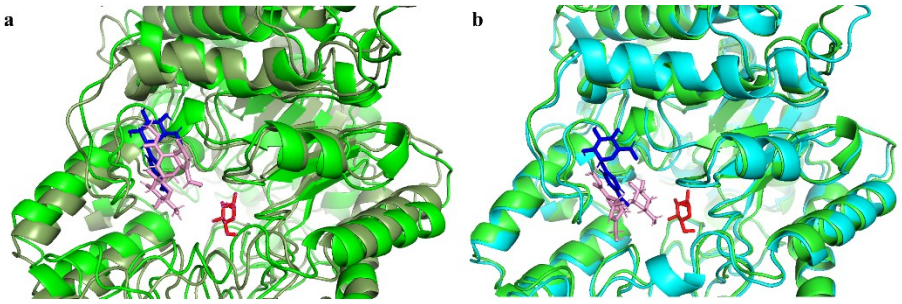

Figure 6. Aligned structures of 6α-, 6β-hydroxygeniposide to PNG-enzyme complexes at the end of simulation (500 picoseconds). PNG: blue color; GLC: red color; 6α- and 6β-hydroxygeniposide: pink.

Table 3. Non-bond interacting energy of isolated iridoids and PNG.

Energy (kJ/mol)	6β-hydroxy geniposide	6α-hydroxy geniposide	PNG
Coul *	-112.851 ± 38.340	-42.323 ± 26.217	-118.112 ± 47.128
LJ**	-124.571 ± 8.795	-88.325 ± 9.108	-12.774 ± 11.959
Total energy	-237.422 ± 35.383	-130.649 ± 28.263	-130.886 ± 46.504

*Coul: Coulombic interaction energy. LJ**: Lennard-Jones interaction energy.

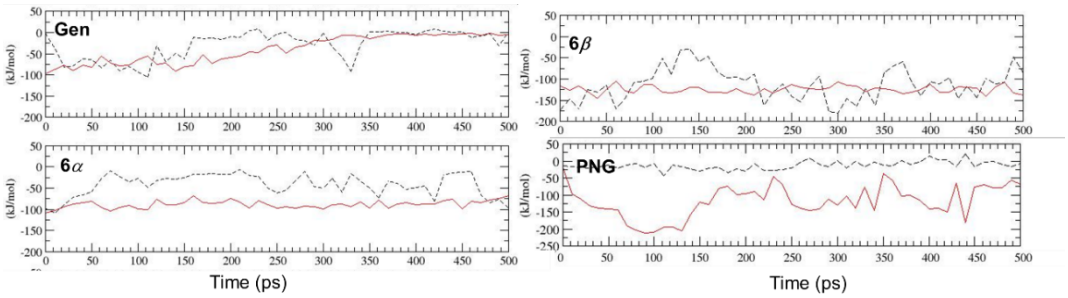

Figure 7. Non-bond interacting energy of isolated iridoids and PNG during simulation (500 ps). gen: geniposide; 6α: 6α-hydroxygeniposide; 6β: 6β-hydroxy geniposide; PNG: p-nitrophenyl-α-D-glucopyranoside. Solid line: Coulombic interaction energy; Dashed line: Lennard-Jones interaction energy.

All the results and analyses suggested that 6β-hydroxygeniposide could compete with substrate PNG and bind to the cavity pocket. The binding was locked in the reaction center and

inhibited the catalysis of the enzyme, which was indicated by a lower RMSF value (Table 2. Figure 4, Supplementary data: Table S4, S5). Meanwhile, the 6α-hydroxygeniposide binding energy was not different from the PNG, therefore, the PNG substrate still approached the reaction center, and the catalysis was conducted.

Although, the anti α-glucosidase activity and molecular dynamic simulation of geniposide, 6α- and 6β-hydroxygeniposide were performed for the first time, our results were compatible with previous studies on molecular docking and dynamic analysis of several α-glucosidase-inhibited compounds such as salvianolic acid A and salvianolic acid C from *Salvia miltiorrhiza* [27]; withanolide A from *Withania somnifera* [28] or Met-Pro-Gly-Pro-Pro (MPGPP) and Phe-Ala-Pro-Ser-Trp (FAPSW) peptides from *Ginkgo biloba* seeds [29].

4. CONCLUSIONS

Three known iridoids geniposide, 6α- and 6β-hydroxygeniposide were extracted from the leaves of *G. jasminoides* collected in Viet Nam. The extremely high anti α-glucosidase activity of 6β-hydroxygeniposide was revealed for the first time, with the potential IC_{50} at 6.38 ± 0.12 μM. By molecular docking combined with molecular dynamics, the inhibition of 6β-hydroxygeniposide was revealed. The 6β-hydroxygeniposide competed and blocked *p*-nitrophenyl-α-D-glucopyranoside substrate reaching the reaction center of the enzyme, which was expressed through lower non-bonding interaction energy and stable binding affinity.

Acknowledgements. This research is funded by Vietnam National Foundation for Science and Technology Development (NAFOSTED) under grant number 104.01-2019.329.

CRediT authorship contribution statement. Nguyen Khac Hung: Investigation, Formal analysis, Methodology. Pham Quang Duong, Chu Van Tan, Nguyen Thi Viet Thanh, Dinh Thi Phuong Anh: Investigation. Cao Duc Tuan: Methodology, Formal analysis. Tran Hong Ngoc, Tran Dai Lam: Formal analysis. Vu Dinh Hoang: Funding acquisition, Formal analysis, Supervision. All authors have read and agreed to the published version of the manuscript.

Declaration of competing interest. The authors declare that they have no known competing financial interests or personal relationships that could have appeared to influence the work reported in this paper.

REFERENCES

1. Pham N. M., Eggleston K. - Diabetes prevalence and risk factors among Vietnamese adults: Findings from community-based screening programs. Diabetes Care, **38**(5) (2015) e77–e78. https://doi.org/10.2337/dc14-3093.
2. Tomic D., Shaw J., Magliano D. - The burden and risks of emerging complications of diabetes mellitus. Nat. Rev. Endocrinol., **18**(9) (2022) 525–539. https://doi.org/10.1038/s41574-022-00690-7.
3. Tran T. D., Tu V. L., Hoang T. M., Dat T. V., Tam D. N. H., Phat N. H., Hung D. T., Huynh H. H., Do T. C., Le H. H., Minh L. H. N. - A review of the In Vitro inhibition of α-amylase and α-glucosidase by chalcone derivatives. Cureus, **15**(4) (2023) e37267. https://doi.org/10.7759/cureus.37267.
4. Brach A. R., Song H. - eFloras: New directions for online floras exemplified by the Flora of China Project. Taxon, **55**(1) (2006) 188–192. https://doi.org/10.2307/25065540.
5. Chen Y., Cheng Y., Tzeng C., Lee Y., Chang Y., Lee S., Tsai C., Chen J., Ceng Tzen J., Chang S. - Peroxisome proliferator-activated receptor activating hypoglycemic effect of *Gardenia jasminoides* Ellis aqueous extract and improvement of insulin sensitivity in steroid induced insulin resistant rats. BMC Complement. Altern. Med., **14**(30) (2014) https://doi.org/10.1186/1472-6882-14-30.

6. Wu S. Y., Wang G. F., Liu Z. Q., Rao J. J., Lu L., Xu W., Wu S. G., Zhang J. J. - Effect of geniposide, a hypoglycemic glucoside, on hepatic regulating enzymes in diabetic mice induced by a high-fat diet and streptozotocin. Acta Pharmacol. Sin., **30**(2) (2009) 202–208. https://doi.org/10.1038/aps.2008.17.
7. Wang G., Wu S., Xu W., Jin H., Zheng G., Li Z., Yuan X., Zhang J., Rao J., Wu S. - Geniposide inhibits high glucose-induced cell adhesion through the NF-κB signaling pathway in human umbilical vein endothelial cells. Acta Pharmacol. Sin., **31** (2010) 953–962. https://doi.org/10.1038/aps.2010.83.
8. Hakamata W., Kurihara M., Okuda H., Nishio T., Oku T. - Design and screening strategies for alpha-glucosidase inhibitors based on enzymological information. Curr. Top. Med. Chem., **9**(1) (2009) 3–12. https://doi.org/10.2174/156802609787354306.
9. Pathania S., Randhawa V., Bagler G. - Prospecting for novel plant-derived molecules of *Rauvolfia serpentina* as inhibitors of aldose reductase, a potent drug target for diabetes and its complications. PLoS One, **8**(4) (2013) e61327. https://doi.org/10.1371/journal.pone.0061327.
10. Shivanika C., Deepak Kumar S., Venkataraghavan R., Pawan T., Sumitha A., Brindha Devi P. - Molecular docking, validation, dynamics simulations, and pharmacokinetic prediction of natural compounds against the SARS-CoV-2 main-protease. J. Biomol. Struct. Dyn., **40**(2) (2022) 585–611. https://doi.org/10.1080/07391102.2020.1815584.
11. Peytam F., Takalloobanafshi G., Saadattalab T., Norouzbahari M., Emamgholipour Z., Moghimi S., Firoozpour L., Bijanzadeh H., Faramarzi M., Mojtabavi S., Rashidi-Ranjbar P., Karima S., Pakraad R., Foroumadi A. - Design, synthesis, molecular docking, and in vitro α-glucosidase inhibitory activities of novel 3-amino-2,4-diarylbenzo[4,5]imidazo[1,2-a]pyrimidines against yeast and rat α-glucosidase. Sci. Rep., **11**(1) (2021) 11911. https://doi.org/10.1038/s41598-021-91473-z.
12. Ali M., Malik K., Zaidi A., Farooq U., Bukhari S., Majeed Z., Mahnashi M., Nawazish S., Abdulwahab A., Alshaibari K. - In-vitro high-throughput library screening-Kinetics and molecular docking studies of potent inhibitors of α-glucosidase. PLoS One, **18**(6) (2023) e0286159. https://doi.org/10.1371/journal.pone.0286159.
13. Eberhardt J., Santos-Martins D., Tillack A., Forli S. - AutoDock Vina 1.2.0: New docking methods, expanded force field, and python bindings. J. Chem. Inf. Model., **61**(8) (2021) 3891–3898. https://doi.org/10.1021/acs.jcim.1c00203.
14. Korb O., Stützle T., Exner T. - PLANTS: Application of Ant Colony Optimization to Structure-Based Drug Design. In *Ant Colony Optimization and Swarm Intelligence*, Springer (2006) 247–258.
15. Mysinger M., Carchia M., Irwin J., Shoichet B. - Directory of Useful Decoys, Enhanced (DUD-E): Better Ligands and Decoys for Better Benchmarking. J. Med. Chem., **55**(14) (2012) 6582–6594. https://doi.org/10.1021/jm300687e.
16. Hajian-Tilaki K. - Receiver Operating Characteristic (ROC) curve analysis for medical diagnostic test evaluation. Casp. J. Intern. Med., **4**(2) (2013) 627–635.
17. O'Boyle N., Banck M., James C., Morley C., Vandermeersch T., Hutchison G. - Open Babel: An open chemical toolbox. J. Cheminform., **3** (2011) 33. https://doi.org/10.1186/1758-2946-3-33.
18. Abraham M., Murtola T., Schulz R., Päll S., Smith J., Hess B., Lindahl E. - GROMACS: High performance molecular simulations through multi-level parallelism from laptops to supercomputers. SoftwareX, **1-2** (2015) 19–25. https://doi.org/10.1016/j.softx.2015.06.001.
19. Lemkul J. - From proteins to perturbed Hamiltonians: A suite of tutorials for the GROMACS-2018 molecular simulation package. Living J. Comput. Mol. Sci., **1**(1) (2019) 1–53. https://doi.org/10.33011/livecoms.1.1.5068.
20. Laskowski R., Swindells M. - LigPlot+: Multiple ligand-protein interaction diagrams for drug discovery. J. Chem. Inf. Model., **51**(10) (2011) 2778–2786. https://doi.org/10.1021/ci200227u.
21. Morota T., Sasaki H., Nishimura H., Sugama K., Chin M., Mitsuhashi H. - Two iridoid glycosides from *Rehmannia glutinosa.* Phytochemistry, **28**(8) (1989) 2149–2153. https://doi.org/10.1016/S0031-9422(00)97934-2.
22. Çalış İ., Weas A., Soliman Yusufoğlu H., Dönmez A., Jensen S. - Iridoid glucosides from *Wendlandia ligustroides* (Boiss. & Hohen.) Blakelock. Saudi Pharm. J., **28**(7) (2020) 814–818. https://doi.org/10.1016/j.jsps.2020.05.009.
23. Velázquez-Fiz M., Díaz-Lanza A., Fernández-Matellano L. - Iridoids from *Plantago lagopus.* Pharm. Biol., **38**(4) (2000) 268–270. https://doi.org/10.1076/1388-0209(200009)3841-AFT268.

24. Hernandez-Rodriguez M., Rosales-Hernandez M. C., Mendieta-Wejebe J. E., Martinez-Archundia M., Basurto J. C. - Current tools and methods in molecular dynamics (MD) simulations for drug design. Curr. Med. Chem., **23**(34) (2016) 3909–3924. https://doi.org/10.2174/0929867323666160530144742.
25. Hevener K., Zhao W., Ball D., Babaoglu K., Qi J., White S., Lee R. - Validation of molecular docking programs for virtual screening against dihydropteroate synthase. J. Chem. Inf. Model., **49**(2) (2009) 444–460. https://doi.org/10.1021/ci800293n.
26. UniProt - Isomaltase (alpha-1,6-glucosidase) from Saccharomyces cerevisiae (strain ATCC 204508 / S288c) (Baker's yeast). https://www.uniprot.org/uniprotkb/P53051/entry (accessed 20 July 2022).
27. Tang H., Zhao D., Xue Z. - Exploring the interaction between Salvia miltiorrhiza and α-glucosidase: Insights from computational analysis and experimental studies. RSC Adv., **8**(44) (2018) 24701–24710. https://doi.org/10.1039/C8RA04772C.
28. Oyewusi H., Wu Y., Safi S., Wahab R., Hatta M., Batumalaie K. - Molecular dynamics simulations reveal the inhibitory mechanism of Withanolide A against α-glucosidase and α-amylase. J. Biomol. Struct. Dyn., **41**(13) (2022) 6203–6218. https://doi.org/10.1080/07391102.2022.2104375.
29. Wang X., Deng Y., Zhang Y., Zhang C., Liu L., Liu Y., Jiang J., Xie P., Huang L. - Screening and evaluation of novel α-glucosidase inhibitory peptides from *Ginkgo biloba* seed cake based on molecular docking combined with molecular dynamics simulation. J. Agric. Food Chem., **71**(27) (2023) 10326–10337. https://doi.org/10.1021/acs.jafc.3c00826.